

Solving nonlinear eigenvalue problems via contour integration and region partitioning

Yuqi Liu¹, Jose E. Roman², and Meiyue Shao^{3,4}

¹*School of Mathematical Sciences, Fudan University, Shanghai 200433, China*

²*D. Sistemes Informàtics i Computació, Universitat Politècnica de València, Camí de Vera s/n, 46022 València, Spain*

³*School of Data Science, Fudan University, Shanghai 200433, China*

⁴*Shanghai Key Laboratory for Contemporary Applied Mathematics, Fudan University, Shanghai 200433, China*

March 18, 2025

Abstract

In this work, we combine Beyn’s method and the recently developed recursive integral method (RIM) to propose a contour integral-based, region partitioning eigensolver for nonlinear eigenvalue problems. A new partitioning criterion is employed to eliminate the need for a problem-dependent parameter, making our algorithm much more robust compared to the original RIM. Moreover, our algorithm can be directly applied to regions containing singularities or accumulation points, which are typically challenging for existing nonlinear eigensolvers to handle. Comprehensive numerical experiments are provided to demonstrate that the proposed algorithm is particularly well suited for dealing with regions including many eigenvalues.

Keywords: Beyn’s method, recursive integral method, region partitioning, nonlinear eigenvalue problem, contour integration

AMS subject classifications (2020). 65F10, 65F15, 65F50

1 Introduction

Given a ξ -dependent matrix $T(\xi): \Omega \rightarrow \mathbb{C}^{n \times n}$, a nonlinear eigenvalue problem (NEP) is to compute the eigenvector $v \in \mathbb{C}^n \setminus \{0\}$ and the corresponding eigenvalue $\lambda \in \Omega$ satisfying

$$T(\lambda)v = 0,$$

where $\Omega \subseteq \mathbb{C}$ is a connected region [12, 27]. In this work, we are particularly interested in the cases where the function $T(\xi)$ is *nonlinear* with respect to ξ . This kind of problems has gained increasing relevance in recent years, and its applications can be found in various disciplines such as fluid dynamics [14, 33], material sciences [1], and computational chemistry [3].

One of the most prevalent applications of NEP in recent years is the calculation of quasi-normal modes of dispersive materials, which is also referred to as QNM analysis [7, 22, 28]. In such applications, magnitudes associated with Maxwell equations are usually discretized by

finite element methods, resulting in NEPs. The eigenvalues of these NEPs contain the damping and frequency of the wave's behavior, which is particularly important for understanding complex materials such as semiconductors and metamaterials. However, to achieve reasonably good accuracy, researchers usually construct physical models with high-order polynomials or rational functions, making numerical computation challenging.

A variety of algorithms can be employed to solve these NEPs, one class of successful methods is that of the Krylov-based algorithms, where the NEP is first approximated and reformulated as a linear eigenvalue problem via companion linearization, which is then solved by Krylov methods. This class of methods has undergone significant developments in recent years, resulting in the emergence of numerous algorithms based on Taylor expansion [19], Chebyshev interpolation [21], and rational approximation [6, 13].

Nevertheless, in many applications, we are concerned with finding all the eigenvalues within a specific region, as we usually do for QNM. In such cases, contour integral-based algorithms, which employ the quadrature rules to approximate the eigenvalues enclosed by a certain contour, make their way into the spotlight. Although these algorithms were originally designed for linear eigenvalue problems [29, 30, 31], some recent developments have extended them to more general nonlinear cases [2, 5, 10, 38].

However, it is important to note that these algorithms are typically designed for cases where only a modest number of eigenvalues are to be computed. Note that, unlike linear eigenvalue problems, the eigenvectors of NEPs are not necessarily linearly independent. As the number of eigenvalues increases, the matrix consisting of the corresponding eigenvectors is more likely to become ill-conditioned, which presents a challenge for both Krylov-based and contour integral-based algorithms.

To address this challenge, a natural idea is to divide the whole region into several smaller ones, and deal with them individually to reduce the number of eigenpairs that need to be handled at each step. In fact, using the idea of partitioning to solve linear symmetric eigenvalue problems is already a well-established approach, with robust mathematical libraries available [23]. This approach employs the theory of spectral density [25] to divide the real axis into several subintervals, and then solve the eigenvalue problem on each subinterval.

As for the nonlinear case, there are also some algorithms based on a similar idea. The reduced subspace iteration (RSI) algorithm [32] is a recently developed Krylov-based solver for NEP. A key distinction between this approach and other Krylov-based algorithms is that, once it approximates the eigenvalues around a certain shift with the Arnoldi process, a K -means algorithm is employed to split the approximate eigenvalues into multiple clusters. The cluster cores are then selected as new shifts, and further Arnoldi processes are implemented on these shifts, respectively, to obtain more accurate solutions. Unlike classical Krylov-based nonlinear solvers, appropriate shifts are selected adaptively without a priori information. Therefore, RSI is particularly well suited for solving problems involving many eigenvalues.

In contrast, the recursive integral method (RIM) [16] is another partitioning algorithm, but using contour integration. This algorithm shares a similar idea to the well-known bisection algorithm for standard symmetric tridiagonal eigenproblems. It uses a quadrature rule-based indicator to determine whether there is any eigenvalue contained in the region of interest. If so, the region is divided into several subregions. The same procedure will be repeated recursively until the subregions are sufficiently small to meet the desired accuracy. Several enhancements have been made to RIM to improve its practicality and cost-effectiveness [15, 17]. A nonlinear implementation is also proposed in [36].

However, in some practical applications, both RSI and RIM face issues of missing eigenvalues. This problem becomes particularly severe when the region of interest contains a large number of eigenvalues or is close to singularities. In applications such as analyzing the resonances of a

material, missing eigenvalues can lead to inaccurate predictions. Therefore, our main goal is to design a more robust algorithm that overcomes this issue.

In this work, we adopt the idea of the RIM but remove the indicators used in that method. Instead, a novel partitioning criterion based on Beyn's method [5] is employed to estimate the information of the region more accurately. The proposed algorithm is capable of handling large-scale problems with many required eigenvalues, robust to singularities, accumulation points, and high multiplicities, and also less prone to missing eigenvalues.

The remainder of this paper is organized as follows. In Section 2, we will briefly introduce the two main components of our algorithm: Beyn's method and the RIM. Then, in Section 3, we will provide a comprehensive description of our proposed new algorithm, including implementation details. Finally, in Section 4, we present comprehensive numerical experiments that demonstrate the excellent performance of our algorithm in specific physical applications.

For simplicity, we have used MATLAB functions `find`, `length`, and `blkdiag` in the pseudocode. Their meanings are as follows:

- `find`: Returns the indices of the elements in an array that satisfy a given condition.
- `length`: Returns the length of an array.
- `blkdiag`: Constructs a block diagonal matrix from the input matrices.

2 Preliminaries

2.1 Beyn's method and quadrature rules

Beyn's method [5] is one of the most well-known contour integral-based nonlinear eigensolvers. To describe this algorithm, we define the zeroth and first moments

$$\mathcal{M}_0 = \frac{1}{2\pi i} \int_{\partial\Omega} T(\xi)^{-1} Z \, d\xi, \quad \mathcal{M}_1 = \frac{1}{2\pi i} \int_{\partial\Omega} \xi T(\xi)^{-1} Z \, d\xi, \quad Z \in \mathbb{C}^{n \times k}.$$

Assuming that there are exactly k eigenvalues of the NEP $T(\lambda)v = 0$ lying within the region Ω , a clever proof provided in [5] states that these eigenvalues, as well as their corresponding eigenvectors, can be obtained by performing a spectral decomposition on the matrix $V_0^* \mathcal{M}_1 W_0 \Sigma_0^{-1}$ for almost any $Z \in \mathbb{C}^{n \times k}$, where $\mathcal{M}_0 = V_0 \Sigma_0 W_0^*$ is the singular value decomposition (SVD) of \mathcal{M}_0 .

However, in numerical implementations, these moments should be approximated by quadrature rules. In this work, to facilitate region partitioning, we adopt a rectangular contour combined with the Gauss–Legendre quadrature rule. Similarly to the classical approach of using the trapezoidal rule on an elliptical contour, the Gauss–Legendre rule on each edge of a polygon has been proven to converge exponentially with respect to the number of quadrature nodes [20, 34].

When applying quadrature rules to the boundary of a rectangular region, we assign $N/4$ quadrature nodes equally to each of its edges. Then, the quadrature nodes and the corresponding weights can be obtained through a transformation of the form

$$\begin{aligned} \xi_{j,s} &= \frac{\tilde{\xi}_j \cdot (b_s - a_s) + (b_s + a_s)}{2}, & \omega_{j,s} &= \frac{\tilde{\omega}_j \cdot (b_s - a_s)}{2}, \\ j &= 0, \dots, \frac{N}{4} - 1, & s &= 0, 1, 2, 3, \end{aligned} \tag{1}$$

where $\tilde{\xi}_j$, $\tilde{\omega}_j$, $j = 0, \dots, N/4 - 1$ are the positions and weights of the standard Gauss–Legendre quadrature rule on the real interval $[-1, 1]$. (Note that $\tilde{\xi}_j$ and $\tilde{\omega}_j$ can be calculated with high

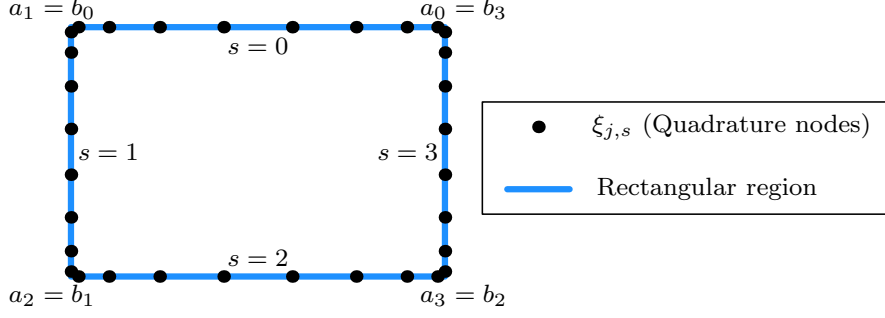


Figure 1: Gauss-Legendre quadrature rule on the boundary of a rectangular region.

Algorithm 1 Beyn’s method with Gauss-Legendre quadrature rule on a rectangular contour.

Input: The parameter-dependent matrix $T(\xi): \Omega \rightarrow \mathbb{C}^{n \times n}$, the initial guess $Z \in \mathbb{C}^{n \times k}$, the number of quadrature nodes N , and the rectangular region of interest Ω

Output: Approximate eigenvalues Λ and eigenvectors V

- 1: **function** $[\Lambda, V] = \text{BeynGL}(Z, \Omega)$
 - 2: Generate nodes $\xi_{j,s}$ and weights $\omega_{j,s}$ on $\partial\Omega$ by (1) for $j = 0, \dots, N/4 - 1, s = 0, 1, 2, 3$
 - 3: $\mathcal{M}_{0,N} \leftarrow \frac{1}{2\pi i} \sum_{s=0}^3 \sum_{j=0}^{N/4-1} \omega_{j,s} T(\xi_{j,s})^{-1} Z$
 - 4: $\mathcal{M}_{1,N} \leftarrow \frac{1}{2\pi i} \sum_{s=0}^3 \sum_{j=0}^{N/4-1} \omega_{j,s} \xi_{j,s} T(\xi_{j,s})^{-1} Z$
 - 5: Singular value decomposition $\mathcal{M}_{0,N} = V_0 \Sigma_0 W_0^*$
 - 6: $\tilde{\mathcal{M}}_{1,N} \leftarrow V_0^* \mathcal{M}_{1,N} W_0 \Sigma_0^{-1}$
 - 7: Eigenvalue decomposition $\tilde{\mathcal{M}}_{1,N} = S \Lambda S^{-1}$
 - 8: $V \leftarrow V_0 S$
 - 9: **end function**
-

accuracy and efficiency by solving a tridiagonal eigenvalue problem [9].) Also, for convenience, we label the four edges with $s = 0, 1, 2, 3$ in a counterclockwise order, and $a_s, b_s \in \mathbb{C}$ are the starting and ending points of the edge s ; see Figure 1.

Consequently, when applying to Beyn’s method, approximate moments read

$$\mathcal{M}_{0,N} = \frac{1}{2\pi i} \sum_{s=0}^3 \sum_{j=0}^{N/4-1} \omega_{j,s} T(\xi_{j,s})^{-1} Z, \quad \mathcal{M}_{1,N} = \frac{1}{2\pi i} \sum_{s=0}^3 \sum_{j=0}^{N/4-1} \omega_{j,s} \xi_{j,s} T(\xi_{j,s})^{-1} Z. \quad (2)$$

For reference, we list Beyn’s method with the Gauss-Legendre quadrature rule in Algorithm 1.

2.2 The recursive integral method

The recursive integral method (RIM) [15, 16, 17, 36] is a nonlinear eigensolver based on contour integration and region partitioning. The idea of RIM is that, for a region $\Omega \subseteq \mathbb{C}$, the operator

$$I_\Omega(z) = \left\| \frac{1}{2\pi i} \int_{\partial\Omega} T(\xi)^{-1} \frac{z}{\|z\|_2} d\xi \right\|_2$$

will return zero for almost any $z \in \mathbb{C}^n, z \neq 0$, if there is no eigenvalue of $T(\xi)$ inside Ω . Therefore, for a region Ω_* , we can determine if Ω_* contains an eigenvalue by evaluating $I_{\Omega_*}(z)$. The regions with $I_{\Omega_*}(z) > 0$ will be divided recursively until the diameter of the currently processed region

Algorithm 2 Recursive integral method (RIM)

Input: Rectangular region of interest Ω , accuracy tolerance for eigenvalues δ_{eig} , classification threshold for the indicator δ_{ind} , and the number of quadrature nodes N

Output: Approximate eigenvalues Λ

```
1: function  $[\Lambda] = \text{RIM}(\Omega)$ 
2:  $\Lambda = []$ 
3: Randomly generate  $z \in \mathbb{C}^n$  with  $\|z\|_2 = 1$ 
4: Generate nodes  $\xi_{j,s}$  and weights  $\omega_{j,s}$  on  $\partial\Omega$  by (1) for  $j = 0, \dots, N/4 - 1, s = 0, 1, 2, 3$ 
5: Compute  $I_{\Omega,N}(z) = \left\| \sum_{s=0}^3 \sum_{j=0}^{N/4-1} \omega_{j,s} T(\xi_{j,s})^{-1} z \right\|_2 / (2\pi)$ 
6: if  $I_{\Omega,N}(z) < \delta_{\text{ind}}$  then
7:   exit % No eigenvalues in  $\Omega$ , return void
8: else if the diameter of  $\Omega$  is larger than  $2 \cdot \delta_{\text{eig}}$  then
9:   Divide  $\Omega$  into  $\Omega_j$  for  $j = 0, \dots, 3$  % by Figure 2
10:  for  $j = 0, \dots, 3$  do
11:     $\Lambda \leftarrow \text{blkdiag}(\Lambda, \text{RIM}(\Omega_j))$  % Not converged yet, divide the region
12:  end for
13: else
14:   $\Lambda \leftarrow$  the center of  $\Omega$  % Converged, return center of  $\Omega$  as approximate eigenvalue
15: end if
16: end function
```

is sufficiently small to meet the accuracy requirement for the eigenvalues. At this point, the algorithm returns the center of that region as an approximate eigenvalue, which is similar to the bisection algorithm used in standard symmetric tridiagonal eigenproblems.

Of course, the contour integration in $I_{\Omega}(z)$ is by no means calculated mathematically. RIM employs an indicator with an N -point quadrature rule

$$I_{\Omega,N}(z) = \left\| \frac{1}{2\pi i} \sum_{j=0}^{N-1} \omega_j T(\xi_j)^{-1} \frac{z}{\|z\|_2} \right\|_2, \quad (3)$$

where ξ_j 's and ω_j 's are some quadrature nodes and weights on $\partial\Omega$. A classification threshold $\delta_{\text{ind}} > 0$ is used to determine partitioning—whenever $I_{\Omega,N}(z) \geq \delta_{\text{ind}}$, we suppose that Ω_* contains at least one eigenvalue, and divide it into several subregions. The framework of the RIM is listed in Algorithm 2.

An advantage of this algorithm is that RIM is able to isolate all the eigenvalues without a priori spectral information [16]. The algorithm can locate the eigenvalues even with only four quadrature nodes, which makes it a powerful tool to solve transmission eigenvalue problems [11, 16].

However, the classification threshold for the indicator δ_{ind} used in Algorithm 2 is highly dependent on the specific problem, making it a tricky task to choose δ_{ind} in practice [36]. A too large δ_{ind} may result in the loss of certain eigenvalues, while a too small one could lead to unnecessary computation of regions that do not actually contain an eigenvalue. Even for the same problem, as subregions become finer during partitioning, the return value of $I_{\Omega,N}(z)$ may vary significantly, making the parameter ineffective and the algorithm inefficient.

Furthermore, the indicator (3) operates on a single vector z , and therefore can only return binary information about the existence or not of eigenvalues. Thus, the algorithm has to increase the search depth in order to ensure that only one eigenvalue is contained in each subregion in the end, which can exponentially increase the computational cost.

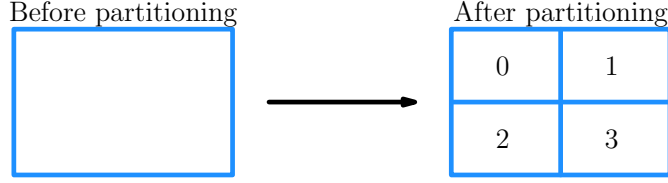


Figure 2: Partitioning pattern.

Remark 1 (How to divide the region). In this paper, we always assume that the region of interest is rectangular. When partitioning, the region is divided into four equal smaller rectangular subregions in a cross-shaped manner; see Figure 2. For convenience, we label these subregions by 0, 1, 2, 3.

3 Proposed algorithm

To improve the RIM, we have two primary goals: to avoid excessive search depth and to eliminate the problem-dependent threshold δ_{ind} .

3.1 RIM by numerical rank

To achieve the first goal, we would like to employ a matrix $Z \in \mathbb{C}^{n \times k_{\text{sub}}}$ for some $k_{\text{sub}} > 1$, instead of using a single vector $z \in \mathbb{C}^n$ in (3). Note that it has been proved in [5] that for almost any Z the rank of the zeroth moment

$$\mathcal{M}_0 = \frac{1}{2\pi i} \int_{\partial\Omega} T(\xi)^{-1} Z \, d\xi$$

is exactly $\min\{k_{\text{sub}}, k\}$, where k is the number of eigenvalues of $T(\xi)$ within Ω . Thus, by estimating the rank of \mathcal{M}_0 , we can determine whether there are eigenvalues within the region and also estimate the number of them.

Therefore, we can divide the region only if \mathcal{M}_0 is of full rank. When \mathcal{M}_0 is rank deficient, it indicates that the region contains less than k_{sub} eigenvalues, and we can apply existing NEP solvers to compute them directly to reduce the excessive search depth which may emerge in RIM.¹ This allows the algorithm to stop earlier, without the need to divide the region into excessively small pieces.

To estimate the rank of \mathcal{M}_0 numerically, a typical approach is to perform a truncated SVD on the approximate moment $\mathcal{M}_{0,N}$ (see (2)) by dropping singular values below a classification threshold δ_{nr} . The rank estimated by this truncated SVD procedure is then taken as the numerical rank of \mathcal{M}_0 . We summarize this modification of RIM in Algorithm 3.

Nevertheless, this approach shares a similar problem with RIM: For different problems, the proper threshold δ_{nr} can be very different, and a poorly chosen δ_{nr} leads to a completely wrong estimate of the rank of \mathcal{M}_0 .

3.2 Recursive Beyn's method

To address the issue of RIM, we have to introduce a more quantifiable criterion to determine whether a region should be further divided. Beginning from Line 6 of Algorithm 3, this time we

¹A similar idea can be found in [36], where Beyn's method is employed to terminate the RIM earlier.

Algorithm 3 The recursive integral method by numerical rank

Input: Rectangular region of interest Ω , classification threshold for numerical rank δ_{nr} , relaxation parameter δ_{relax} , maximum number of eigenvalues of each subregion k_{sub} , the number of quadrature nodes N , and a high performance NEP solver `NEPsolver()` for small-scale problems

Output: Approximate eigenvalues Λ

```

1: function  $[\Lambda] = \text{RIMNR}(\Omega)$ 
2:  $\Lambda = []$ 
3: Randomly generate  $Z \in \mathbb{C}^{n \times k_{\text{sub}}}$ 
4: Generate nodes  $\xi_{j,s}$  and weights  $\omega_{j,s}$  on  $\partial\Omega$  by (1) for  $j = 0, \dots, N/4 - 1, s = 0, 1, 2, 3$ 
5:  $\mathcal{M}_{0,N} \leftarrow \frac{1}{2\pi i} \sum_{s=0}^3 \sum_{j=0}^{N/4-1} \omega_{j,s} T(\xi_{j,s})^{-1} Z$ 
6: Singular value decomposition  $\mathcal{M}_{0,N} = V_0 \Sigma_0 W_0^*$ 
7:  $k_{\text{in}} \leftarrow \text{length}(\text{find}(\text{diag}(\Sigma_0) > \delta_{\text{nr}}))$     % The number of singular values larger than  $\delta_{\text{nr}}$ 
8: if  $k_{\text{in}}/k_{\text{sub}} < \delta_{\text{relax}}$  then
9:    $\Lambda \leftarrow \text{NEPsolver}(\Omega)$     % Few eigenvalues in  $\Omega$ , use NEPsolver
10: else
11:   Divide  $\Omega$  into  $\Omega_j$  for  $j = 0, \dots, 3$     % by Figure 2
12:   for  $j = 0, \dots, 3$  do
13:      $\Lambda \leftarrow \text{blkdiag}(\Lambda, \text{RIMNR}(\Omega_j))$     % Too many eigenvalues, divide the region
14:   end for
15: end if
16: end function

```

continue on Beyn's method, i.e., Algorithm 1, until the approximate eigenvalues Λ are obtained. Then, instead of using the numerical rank, we employ the number of Λ lying within the region Ω , as the approximate rank of \mathcal{M}_0 . The new algorithm, referred to as recursive Beyn's method, is listed in Algorithm 4.

This approach eliminates the necessity for a classification threshold such as δ_{ind} and δ_{nr} , which are highly problem-dependent and not robust, resulting in a more flexible partitioning criterion. Furthermore, it can be observed from Algorithm 1 that, by the time $\mathcal{M}_{0,N}$ is computed, the majority of the computational cost of Beyn's method has already been incurred. The remaining steps to complete a full run of Beyn's method are of low computational complexity, which means the overhead introduced is very low.

Remark 2. In both Algorithms 3 and 4, a relaxation parameter $0 < \delta_{\text{relax}} \leq 1$ is introduced. We use $k_{\text{in}}/k_{\text{sub}} \geq \delta_{\text{relax}}$ instead of $k_{\text{in}} = k_{\text{sub}}$ as the criterion to decide whether to proceed with an additional level of partitioning. A $\delta_{\text{relax}} < 1$ can help avoid the potential risk of missing eigenvalues in some challenging cases, at the cost of increasing the search depth of the algorithm. Note that, unlike δ_{ind} in RIM, the value used for the parameter δ_{relax} will not influence the correctness of the algorithm.

Remark 3. In Algorithm 4, we introduce another parameter d_{max} to limit the depth of recursion. The algorithm stops when the maximum search depth d_{max} is reached. Unexploited subregions can be marked for future processing, if necessary. This enables the algorithm to deal with difficult regions such as those containing singularities and eigenvalues with high multiplicities.

Remark 4. It is worth noting that Algorithm 2, as originally defined in [16], as well as Algorithm 3, can only return eigenvalues. Further computations should be done if the eigenvectors are also required. In contrast, Algorithm 4 can return the corresponding eigenvectors at the same time, since Beyn's method is used.

Algorithm 4 The recursive Beyn's method

Input: Rectangular region of interest Ω , accuracy tolerance for eigenpairs δ_{res} , maximum number of eigenvalues of each subregion k_{sub} , relaxation parameter δ_{relax} , the number of quadrature nodes N , and the maximum search depth d_{max}

Output: Approximate eigenvalues Λ and eigenvectors V

```
1: function  $[\Lambda, V] = \text{RBM}(d_{\text{max}}, \Omega)$ 
2:  $V \leftarrow []$ ,  $\Lambda \leftarrow []$ 
3: Randomly generate  $Z \in \mathbb{C}^{n \times k_{\text{sub}}}$ 
4:  $[\Lambda_{\text{tmp}}, V_{\text{tmp}}] = \text{BeynGL}(Z, \Omega)$  % BeynGL is defined in Algorithm 1
5:  $\text{idx} = \text{find}(\Lambda_{\text{tmp}} \in \Omega)$  % Identify eigenpairs in  $\Omega$ 
6:  $\Lambda_{\text{tmp}} \leftarrow \Lambda_{\text{tmp}}(\text{idx}, \text{idx})$ ,  $V_{\text{tmp}} \leftarrow V_{\text{tmp}}(:, \text{idx})$ 
7:  $k_{\text{in}} \leftarrow \text{length}(\text{idx})$ 
8: Check convergence on  $[\Lambda_{\text{tmp}}, V_{\text{tmp}}]$ 
9: if  $k_{\text{in}}/k_{\text{sub}} < \delta_{\text{relax}}$  and  $[\Lambda_{\text{tmp}}, V_{\text{tmp}}]$  converged then % Converged, save the solutions
10:  $V \leftarrow V_{\text{tmp}}$ ,  $\Lambda \leftarrow \Lambda_{\text{tmp}}$ 
11: else if  $d_{\text{max}} > 0$  then % by Figure 2
12: Divide  $\Omega$  into  $\Omega_j$  for  $j = 0, \dots, 3$ 
13: for  $j = 0, \dots, 3$  do
14:  $[\Lambda_{\text{tmp}}, V_{\text{tmp}}] = \text{RBM}(d_{\text{max}} - 1, \Omega_j)$ 
15:  $V \leftarrow [V, V_{\text{tmp}}]$ ,  $\Lambda \leftarrow \text{blkdiag}(\Lambda, \Lambda_{\text{tmp}})$  % Not converged, divide the region
16: end for
17: end if
18: end function
```

3.3 Accelerate the linear solver with infinite GMRES

Infinite GMRES (infGMRES) [18] is a recently proposed algorithm for solving parameterized linear systems

$$T(\xi)x = b, \quad b \in \mathbb{C}^n, \quad T(\xi): \Omega \rightarrow \mathbb{C}^{n \times n}, \quad \Omega \subseteq \mathbb{C},$$

on $\xi = \xi_0, \xi_1, \dots$, altogether efficiently. In brief, infGMRES uses Taylor expansion and companion linearization to transform the problem into solving another parameterized linear system

$$(I - \xi \mathcal{L}_0^{-1} \mathcal{L}_1) \tilde{y} = \tilde{b}, \quad \tilde{b} \in \mathbb{C}^{mn}, \quad \mathcal{L}_0, \mathcal{L}_1 \in \mathbb{C}^{mn \times mn},$$

on $\xi = \xi_0, \xi_1, \dots$, where $m \in \mathbb{N}$ is a parameter related to the order of the Taylor expansion. Since the Krylov subspaces generated by $I - \xi_j \mathcal{L}_0^{-1} \mathcal{L}_1$ with different ξ_j 's are the same, the linear systems can be solved by a single Arnoldi process. In [26], we have employed infGMRES to accelerate the contour integral-based nonlinear eigensolvers. This idea can also be applied here to enhance the efficiency of recursive Beyn's method.

However, it is proved in [18] that the accuracy of infGMRES is influenced by the distance between the points to be solved and the point employed for the Taylor expansion (that is, the expansion point). In order to ensure accuracy, it is often necessary to distribute multiple expansion points. To this end, the simplest idea is to first place a uniform grid over the region Ω , use these grid points as expansion points to employ infGMRES, and store the corresponding Arnoldi and Hessenberg matrices. Then, whenever a linear system is to be solved in Line 4, Algorithm 4, we simply choose the nearest expansion point, and utilize the precomputed infGMRES results at that point for efficient solving. In Section 4.4, several numerical examples are provided to illustrate the performance of employing infGMRES in this way.

We remark that our application of infGMRES here is just heuristic. In addition to the distance we have just mentioned, the accuracy of infGMRES is also influenced by multiple factors, such as the singularities of T . As a result, in practical applications, it is often difficult to determine in advance how to distribute the expansion points to ensure that all linear systems are solved accurately.

4 Numerical experiments

In this section, we employ recursive Beyn's method (Algorithm 4) to solve several NEPs in physical applications. All numerical experiments were carried out using MATLAB R2023b on a Linux server with two 16-core Intel Xeon Gold 6226R 2.90 GHz CPUs and 1024 GB of main memory. The convergence criterion for an approximate nonlinear eigenpair $(\hat{\lambda}, \hat{v})$ is

$$\|T(\hat{\lambda})\hat{v}\|_2 \leq \delta_{\text{res}} \cdot \|T(\hat{\lambda})\|_2 \|\hat{v}\|_2,$$

where δ_{res} is a user-specified tolerance. Unless otherwise stated, all test results presented in this section have achieved an accuracy of $\delta_{\text{res}} = 10^{-12}$, and the relaxation parameter δ_{relax} in Algorithm 4 is always set to 0.8.

4.1 Test problems

We begin with a brief introduction to three test NEPs, describe their respective properties and challenges, and present the overall performance of our algorithm on these problems.

4.1.1 The gun problem

The **gun** problem [24] is one of the most popular test problems for nonlinear eigensolvers [32, 35]. The problem is derived from the electromagnetic modeling of waveguide loaded accelerator cavities. With a nonlinear boundary condition, the physical problem can be discretized by the finite element method to

$$\begin{aligned} & \left(A_0 - \lambda A_1 + i\sqrt{\lambda - \kappa_{c,1}^2} A_2 + i\sqrt{\lambda - \kappa_{c,2}^2} A_3 \right) v = 0, \\ & \kappa_{c,1}, \kappa_{c,2} \in \mathbb{R}, \quad A_0, A_1, A_2, A_3 \in \mathbb{R}^{9956 \times 9956}. \end{aligned} \tag{4}$$

In this work, we generate the **gun** problem from the NLEVP collection [4], and take the region of interest to be the square centered at $(250^2, 0)$ with side length $2 \cdot (300^2 - 200^2)$ [35].

The result of solving the problem using recursive Beyn's method can be found in Figure 3. The grid of subregions and the approximate eigenvalues are shown in the figure. All 22 eigenpairs in the region of interest are found and computed with a relative residual below 10^{-12} . Note that the square roots in (4) are both defined by the principal branch and therefore lead to a branch cut $(-\infty, \kappa_{c,2}^2]$ lying close to the boundary of the region. This introduced some challenges to the subregions on the left-hand side. However, our algorithm successfully identified all the eigenvalues accurately.

4.1.2 The photonics_1 problem

To better demonstrate the performance of our algorithm in practical applications, we provide two recently proposed problems from quasinormal modes analysis (QNM). The physical model [7, 8] being considered is illustrated in Figure 4, an infinite number of rods are evenly distributed along

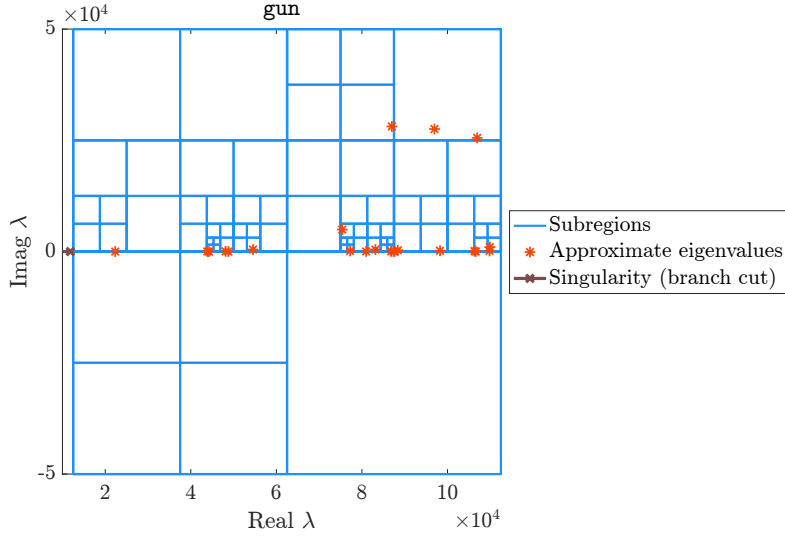


Figure 3: Using recursive Beyn’s method to solve the **gun** problem. The region of interest is $[1.25 \times 10^4, 1.125 \times 10^5] \times [-5 \times 10^4, 5 \times 10^4]$ in the complex plane. The parameters are set as: maximum eigenvalues in each subregion $k_{\text{sub}} = 5$, number of quadrature nodes on each segment $N = 32$, and maximum search depth $d_{\text{max}} = 6$. All 22 eigenvalues as well as their corresponding eigenvectors are found. The branch cut $(-\infty, 108.8774^2]$ is indicated by a line with a cross mark on its endpoint.

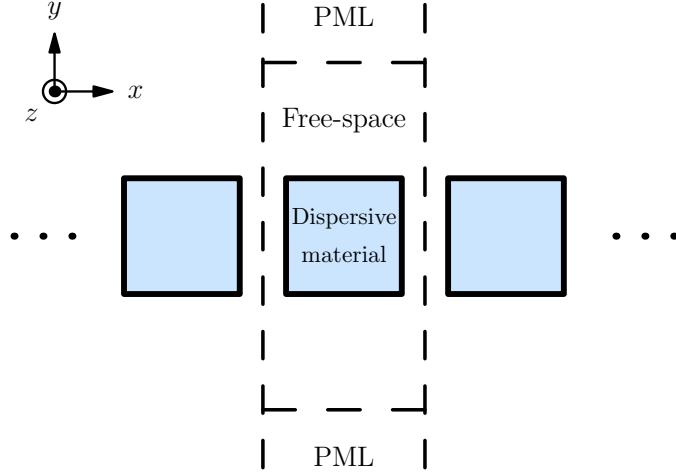


Figure 4: Geometric distribution of the **photronics_1** and **photronics_2** problems.

the x -axis, and their gaps are filled by free-space. Then, along the y -axis, the unbounded domain is handled using the standard Cartesian Perfectly Matched Layer (PML) technique. Additionally, for simplicity, the system is assumed to be invariant along the z -axis.

For the **photronics_1** problem, we take the dispersive material to be gold, and employ the

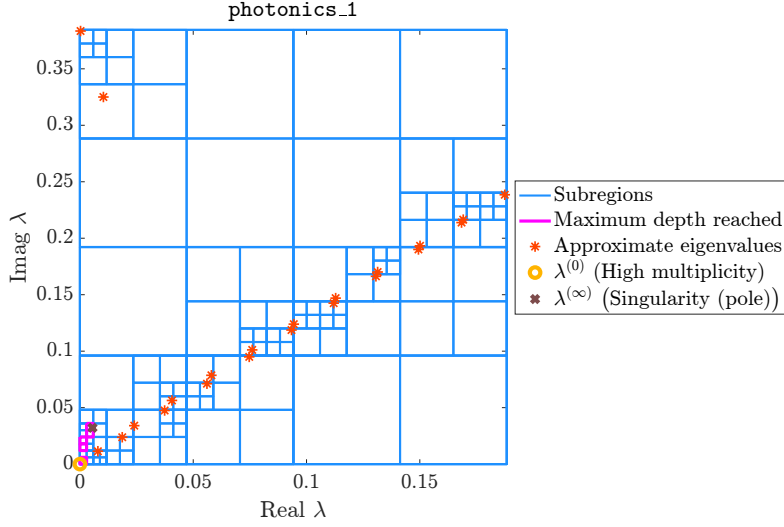


Figure 5: Using recursive Beyn’s method to solve the **photonics_1** problem. The region of interest is $[0, 0.188365] \times [0, 0.384419]$ in the complex plane. The parameters are set as: maximum eigenvalues in each subregion $k_{\text{sub}} = 5$, number of quadrature nodes on each segment $N = 32$, and maximum search depth $d_{\text{max}} = 6$. A total of 22 different nonzero eigenvalues as well as their corresponding eigenvectors are found. The eigenvalue with high multiplicity $\lambda^{(0)}$ and the pole $\lambda^{(\infty)}$ are also marked in the figure.

permittivity model from [8]. Then, the expression for the permittivity reads

$$\varepsilon_p(i\omega) = \varepsilon_\infty + \frac{\alpha_1}{(i\omega) - \beta_1} + \frac{\bar{\alpha}_1}{(i\omega) - \bar{\beta}_1}, \quad \varepsilon_\infty, \alpha_1, \beta_1 \in \mathbb{C},$$

where ω is the (complex) frequency of the electric wave. Using the finite element method, we can discretize Maxwell’s equations on the system to obtain the rational eigenvalue problem

$$(A_0 + \lambda^2 A_1 + \lambda^2 \cdot \varepsilon_p(\lambda) A_2) v = 0, \quad A_0, A_1, A_2 \in \mathbb{C}^{20363 \times 20363}. \quad (5)$$

Solving (5) by recursive Beyn’s method on the region of interest $[0, 0.188365] \times [0, 0.384419]$ leads to Figure 5.

There are two main challenges to this problem:

1. $\varepsilon_p(\lambda^{(0)}) = 0$ or $\lambda^{(0)} = 0$: This means that the permittivity of the material or the electric field itself becomes zero when $\lambda = \lambda^{(0)}$. Physically, this solution is trivial. However, numerically, this eigenvalue usually has an extremely high algebraic multiplicity, which can cause common numerical algorithms to waste excessive computational resources at this meaningless point [7].
2. $\varepsilon_p(\lambda^{(\infty)}) = \infty$: This is a pole of the rational function ε_p . Numerical solutions may be inaccurate near this point.

In addition to the difficulties mentioned above, there is another common challenge for various contour integral-based eigensolvers — the eigenvalues near the contour. When such eigenvalues exist, either inside or outside the region, the quadrature rules are typically observed to be inaccurate [20], resulting in the risk of missing eigenvalues or computing eigenvalues with large errors/slow convergence.

Note from Figure 5 that five subregions are marked as unexploited when the maximum depth 6 is reached (marked in magenta). Although three of them are due to numerical errors, the other two subregions capture the two difficult points, $\lambda^{(0)}$ and $\lambda^{(\infty)}$, respectively. However, we remark that the eigenvalues lying close to $\lambda^{(0)}$, $\lambda^{(\infty)}$, or the boundary of the region of interest, are still calculated with a relative residual below 10^{-12} .

4.1.3 The photonics_2 problem

For the `photonics_2` problem, we consider an even more complicated model from [7]. With the same geometric model as in Figure 4, we use a Drude model for the permittivity — a real-coefficient rational function with respect to $i\omega$ as

$$\varepsilon_d(i\omega) = \varepsilon_\infty - \frac{\omega_d^2}{-(i\omega)^2 + \gamma_d(i\omega)}, \quad \varepsilon_\infty, \omega_d, \gamma_d \in \mathbb{R}, \quad (6)$$

where ω is the (complex) frequency of the electric wave.

Employing all the parameters used in [7] with a finite-element mesh with 1183 elements, we obtain the NEP

$$(A_0 + \lambda^2 A_1 + \lambda^2 \cdot \varepsilon_d(\lambda) A_2) v = 0, \quad A_0, A_1, A_2 \in \mathbb{C}^{6667 \times 6667}. \quad (7)$$

This time, to analyze the quasinormal modes of this system, we aim to compute the eigenvalues within $\lambda \in [0, 0.1] \times [0.0005, 4]$ and their corresponding eigenvectors v . The output of our algorithm on this problem is illustrated in Figure 6.

The problem `photonics_2` is more difficult than `photonics_1`, although the dimension of the former is only about a third of the latter. This is because the region of interest now contains almost 200 different eigenvalues. And, in addition to the previously mentioned difficulties with $\lambda^{(0)}$ (where $\varepsilon_d(\lambda^{(0)}) = 0$ or $\lambda^{(0)} = 0$) and $\lambda^{(\infty)}$ (where $\varepsilon_d(\lambda^{(\infty)}) = \infty$), there is also:

3. $\varepsilon_d(\lambda^{(-1)}) = -1$: $\lambda^{(-1)}$ is an accumulation point of the NEP (7). The eigenvalues concentrated around it correspond to the plasmonic resonances, which means their eigenvectors, or electric field, show a significant oscillation on the interface of the Drude material. These eigenpairs are also not of interest.

It can be observed from the figure that, with a maximum search depth of 8, both $\lambda^{(0)}$ and $\lambda^{(-1)}$ are located by the algorithm. Although the pole $\lambda^{(\infty)} = 0.05$ lies close to the boundary of the region of interest, 197 eigenpairs are computed with a relative residual below 10^{-12} .

4.2 Comparison among different partitioning criteria

In this subsection, we test whether the proposed algorithm can accurately reflect the number of eigenvalues within a region. For comparison, recursive Beyn's method is applied to three different test regions on the `photonics_1` problem; see Figure 7. The three test regions are all taken from the subregions generated during the process of recursive Beyn's method, i.e., from Figure 5.

There are several differences across these regions. Region 3 contains an eigenvalue, while Regions 1 and 2 do not contain any eigenvalue. Another important difference is that there is an eigenvalue lying extremely close to the boundary between Regions 2 and 3, posing a challenge for the contour integration on Regions 2 and 3.

The number of eigenvalues estimated by recursive Beyn's method is plotted at the bottom-right corner of Figure 8. It can be observed that the proposed algorithm accurately estimates the number of eigenvalues on all three test regions, even when only a few quadrature nodes are used.

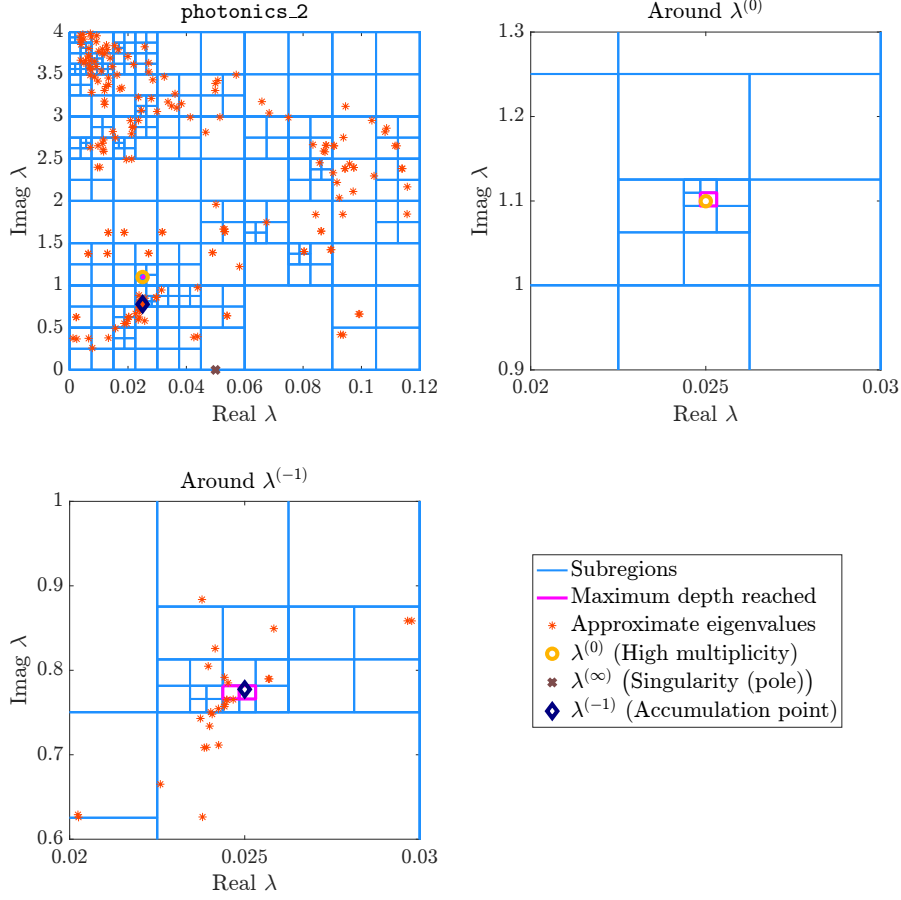


Figure 6: Using recursive Beyn's method to solve the **photonics_2** problem. The region of interest is $[0, 0.12] \times [0.0005, 4]$ in the complex plane. The parameters are set as: maximum eigenvalues in each subregion $k_{\text{sub}} = 20$, number of quadrature nodes on each segment $N = 512$, and maximum search depth $d_{\text{max}} = 8$. A total of 197 different eigenvalues as well as their corresponding eigenvectors are found. The eigenvalue with high multiplicity $\lambda^{(0)}$, the plasmonic resonance $\lambda^{(-1)}$, and the pole $\lambda^{(\infty)}$ are also marked in the figure. To provide a clear picture, we zoom in near $\lambda^{(0)}$ and $\lambda^{(-1)}$.

Three other partitioning methods are also plotted in Figure 8 for comparison. The top-left image is the output of the RIM's indicator $I_{\Omega, N}(z)$. To make our experiments more convincing, we also include the RIM's double indicator

$$I_{\Omega, N}^d(z) = \left\| \frac{1}{2\pi i} \sum_{j=0}^{N-1} \omega_j T(\xi_j)^{-1} \frac{\sum_{j=0}^{N-1} \omega_j T(\xi_j)^{-1} z}{\left\| \sum_{j=0}^{N-1} \omega_j T(\xi_j)^{-1} z \right\|_2} \right\|_2, \quad (8)$$

at the top-right. This indicator, which is also proposed in [16], performs the contour integration twice, and is declared to be more robust than $I_{\Omega, N}(z)$. Finally, the largest singular value of $\mathcal{M}_{0, N}$, i.e., $\|\mathcal{M}_{0, N}\|_2$, is plotted at the bottom-left corner, which reflects the efficiency of Algorithm 3. Remember that Algorithm 3 estimates the number of eigenvalues in a region by truncating its SVD. Thus, we expect to see $\|\mathcal{M}_{0, N}\|_2$ large on Region 3, and small on Regions 1 and 2.

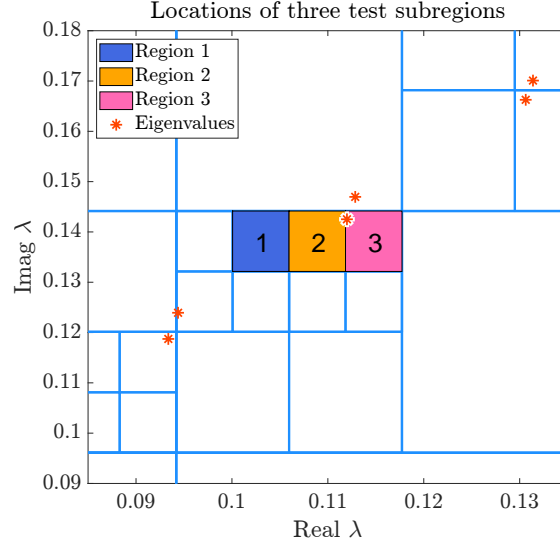


Figure 7: Three test regions. All these regions are chosen from subregions in Figure 5.

Note from Figure 8 that all three comparative experiments perform well on Regions 1 and 3. For Region 1, all three comparative experiments show an exponential decline to 0, indicating that no eigenvalue is included. And for Region 3, which includes one eigenvalue, the trend in all cases is non-decaying with respect to the increase of N , which is a signal for existence of eigenvalues.

Nevertheless, when applied to Region 2, these three methods are no longer reliable. It can be seen that applying them to Regions 2 and 3 gives almost the same result, even though there is no eigenvalue in Region 2. Comparing on Regions 1 and 2, the RIM's indicators and the truncated SVD may return significantly different values for subregions with the same number of eigenvalues, which is zero in our example. Therefore, using a fixed classification threshold δ_{ind} or δ_{nr} to determine partitioning is not reliable.

4.3 Comparison with RSI and RIM

As comparisons, we use two recently proposed partitioning-based nonlinear eigensolvers, RIM and RSI, to solve the `photonics_1` problem.

4.3.1 Using RSI to solve `photonics_1`

Unlike our algorithm, the reduced subspace iteration (RSI) algorithm [32] is a Krylov-based eigensolver. Instead of directly partitioning the region, it achieves partitioning by splitting the shift into several different shifts distributed in the region. Then, the Arnoldi process is employed on each shift to obtain the eigenvalues of the whole region.

The RSI code is provided in [32]. We made slight modifications to the code, enabling the approximate model of RSI to be applied to elliptical regions. The result of using RSI to solve the `photonics_1` problem is illustrated in Figure 9.²

²The nonlinear function $T(\xi)$ is interpolated in RSI. The region of rational approximation and rational quadrature nodes marked in Figure 9 are for this use. For a detailed explanation, see [32].

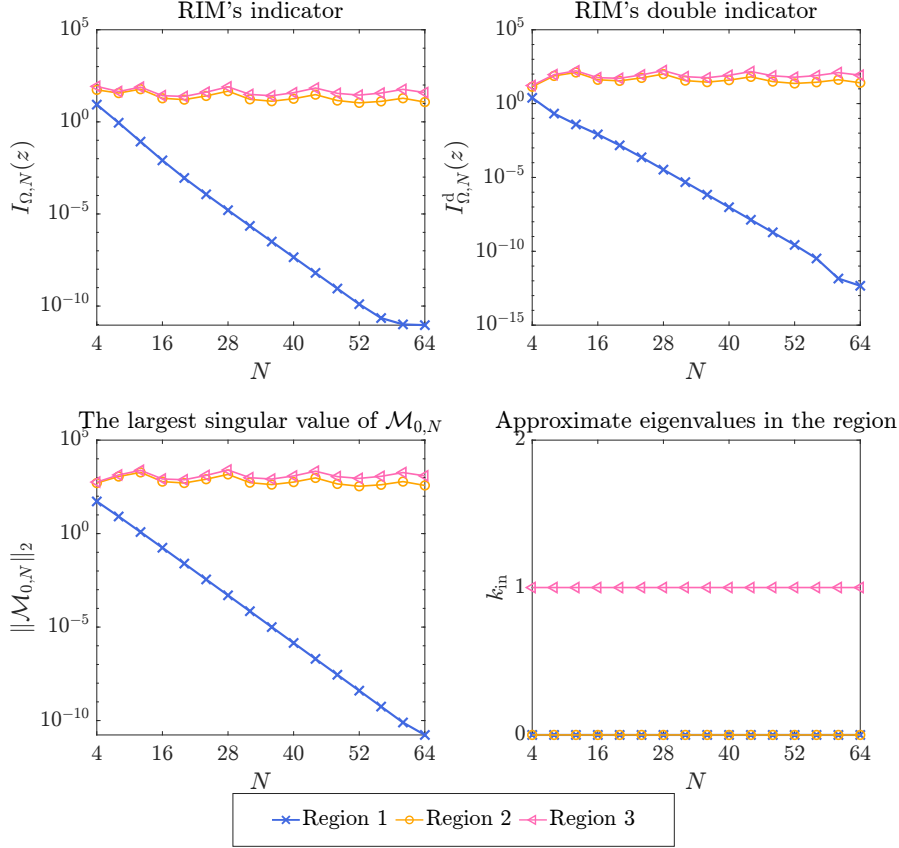


Figure 8: The performance of four partitioning criteria on three different regions in Figure 7.

All 241 eigenvalues obtained by RSI are trivial, since they concentrate around the zero eigenvalue $\lambda^{(0)}$, which means that computational resources are severely wasted trying to determine the eigenvalue with high multiplicity. Nevertheless, the shifts generated by RSI still capture the distribution pattern of eigenvalues within the region; see the shifts and the approximate eigenvalues from RBM in Figure 9. However, the pole $\lambda^{(\infty)}$ destroys the interpolation accuracy of RSI, making it fail to calculate the interior eigenvalues accurately.

4.3.2 Using RIM to solve photonics_1

The recursive integral method (RIM) [16] has already been introduced in Section 2.2. Before presenting the experiments, let us specify the parameters used in our implementation. The RIM's double indicator (8) is employed with a Gauss–Legendre quadrature rule on a rectangular contour. Both the block size $k_{\text{sub}} = 5$ and the number of quadrature nodes on each segment $N = 32$ are set equal to those used in Figure 5 for fairness. However, the target accuracy is set to 10^{-3} to save computational resources. The result is plotted in Figure 10.

Intuitively, RIM appears to have successfully identified the approximate locations of all eigenvalues. In fact, RIM is used for solving similar photonic problems in [37], and shows a satisfactory performance when only a relatively low precision is needed. However, a closer look (see Figure 10 right) reveals that two approximate eigenvalues are calculated around each eigenvalue of

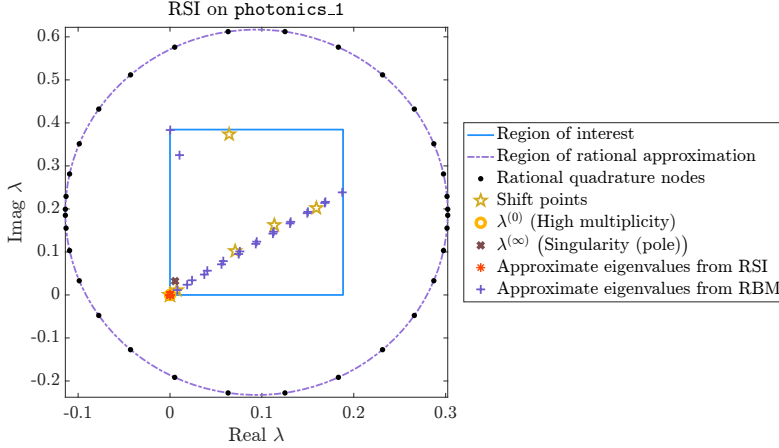


Figure 9: Use of the reduced subspace iteration (RSI) algorithm to solve the `photonics_1` problem. We used a modified version of the code provided in [32] to set the region of rational approximation to be elliptical disks instead of circular disks. The convergence threshold is set to 10^{-12} . The region of rational approximation, the rational quadrature nodes, and five shifts found and used by RSI are marked in the figure. The approximate eigenvalues generated by recursive Beyn’s method (RBM) are also marked in the figure for comparison.

`photonics_1`. This occurs because the indicator returns large values in every subregion around an eigenvalue, which means the indicator can hardly locate the subregions containing eigenvalues accurately. When comparing to Figure 5, it can be observed that the RIM performs unnecessary partitioning in many regions that do not contain any eigenvalue, leading to a waste of computational resources. RIM performs even worse near the pole $\lambda^{(\infty)}$, returning many spurious eigenvalues.

4.4 Implementation with infinite GMRES

In this subsection we illustrate the acceleration effect of infGMRES on recursive Beyn’s method. All three test example, `gun`, `photonics_1`, and `photonics_2`, are solved with infGMRES on a uniform grid of expansion points. The comparison of time consumed is presented in Table 1.

As an example, the result of using recursive Beyn’s method with infGMRES to solve `photonics_1` is shown in Figure 11. We use 12×12 uniformly distributed expansion points, except the point at the origin. Both the approximate eigenvalues and the difficult points $\lambda^{(0)}$ and $\lambda^{(\infty)}$ are found. However, only $143 \times 5 = 715$ LU decompositions on 20363×20363 matrices are needed, and the time consumed is only about $2/3$.

However, as we mentioned before, selecting suitable expansion points to ensure accurate results from infGMRES is challenging. As can be observed in Table 1, some eigenvalues are *missed* due to the inaccuracy of infGMRES. This is partly because infGMRES can hardly solve linear systems near the pole $\lambda^{(\infty)}$ accurately. In fact, it is observed that, even increasing the number of expansion points helps little to improve the accuracy of the solutions of the linear systems near singularities. Therefore, applying infGMRES in intricate regions is technically challenging, and further investigation is needed to make it robust.

However, since our algorithm continuously subdivides the region locally, generating a large number of quadrature nodes and linear systems, there is still significant potential for performance improvement by infGMRES. The linear case of this technique is discussed in [15].

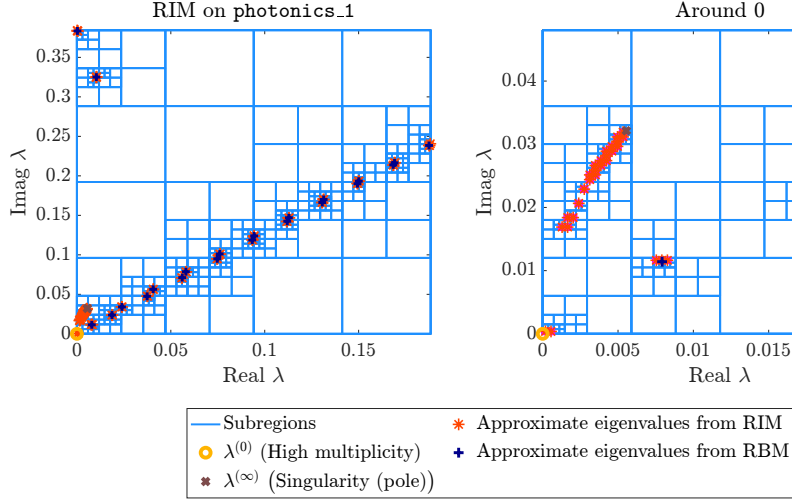


Figure 10: Use of the recursive integral method (RIM) to solve the `photonics_1` problem. We use RIM’s double indicator (8) with a 32-point Gauss–Legendre quadrature rule. The convergence threshold is set to 10^{-3} , to save computational resources, while all other parameters match the ones used in [16]. The approximate eigenvalues generated by recursive Beyn’s method (RBM) are also marked in the figure for comparison.

Table 1: Using infinite GMRES to accelerate recursive Beyn’s method. The columns labeled by ‘Subregions’ and ‘Linear systems’ in the table are the total number of subregions generated and the linear systems solved during the process of recursive Beyn’s method, respectively. The number of infGMRES expansion points is also shown in the table. All other parameters, e.g., d_{\max} , N , and δ_{res} , are the same as in the experiments in Section 4.1. As results, we present the time consumed by infGMRES, the total solving time, and also the number of eigenvalues found.

Problem	InfGMRES	Subregions	Linear systems	Expansion points	InfGMRES time (s)	Total time (s)	Eigenvalues found
gun	w/o	93	14,880	-	-	1066	22
	with	157	25,120	25	132	276	22
photonics_1	w/o	161	25,760	-	-	1488	22
	with	165	26,400	143	501	1023	22
photonics_2	w/o	365	3,737,600	-	-	9340	197
	with	713	7,301,120	240	2842	7646	178

5 Conclusion

In this work, we propose a contour integral-based, region partitioning nonlinear eigensolver, i.e., recursive Beyn’s method, by combining Beyn’s method and the RIM. In this algorithm, we replace the RIM’s indicator with an estimate of the number of eigenvalues to determine whether a region should be further subdivided. This not only avoids the algorithm’s reliance on problem-dependent parameters, but also improves the accuracy of the region partitioning. As a result, the algorithm almost never wastefully subdivides regions that do not contain eigenvalue, which can save computational resources. Furthermore, unlike the RIM algorithm, which requires a postprocessing stage to compute eigenvectors, our recursive Beyn’s method computes both the eigenvalues and the corresponding eigenvectors simultaneously.

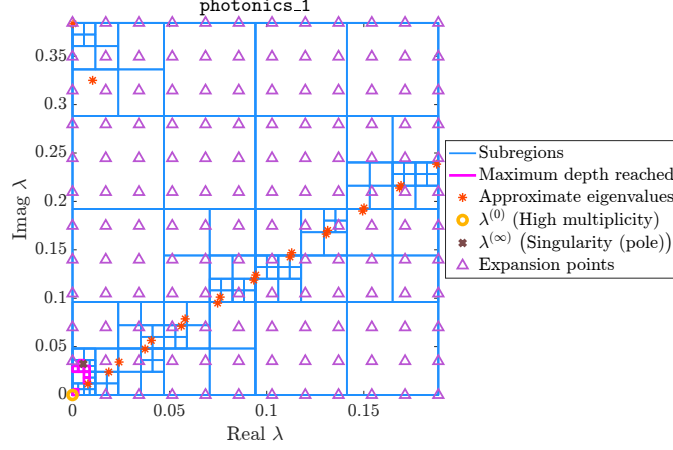


Figure 11: Using recursive Beyn’s method with infGMRES to solve the **photonics_1** problem. The region of interest and the parameters k_{sub} , N , and d_{max} are set equal to the ones used in Figure 5. The expansion points of infGMRES are distributed on a 12×12 uniform grid on the region of interest, except the point at the origin (0). Same as Figure 5, all 22 eigenvalues are found and computed with a relative residual below 10^{12} . The difficult points $\lambda^{(0)}$ and $\lambda^{(\infty)}$ are also located.

In terms of experimental results, the proposed algorithm can accurately identify all eigenpairs, even for the cases when the region of interest is challenging with singularities, high-multiplicity eigenvalues, and accumulation points contained, which can be beneficial for solving certain problems in quasi-normal mode analysis.

At the end of the paper, we also heuristically introduced the idea of using infGMRES to accelerate the algorithm. One of the priorities of our future work will be to adaptively apply infGMRES to our algorithm, further reducing its computational time and enhancing its adaptability to various applications.

Acknowledgments

Y. Liu and M. Shao were partly supported by the National Natural Science Foundation of China under grant No. 92370105. J. E. Roman was partially supported by grants PID2022-139568NB-I00 and RED2022-134176-T funded by MCIN/AEI/10.13039/501100011033 and by “ERDF A way of making Europe”. This work was partly carried out while Y. Liu was visiting Universitat Politècnica de València.

References

- [1] Juan C. Araujo C., Carmen Campos, Christian Engström, and Jose E. Roman. Computation of scattering resonances in absorptive and dispersive media with applications to metal-dielectric nano-structures. *J. Comput. Phys.*, 407:109220, 2020. doi:10.1016/j.jcp.2019.109220.

- [2] Junko Asakura, Tetsuya Sakurai, Hiroto Tadano, Tsutomu Ikegami, and Kinji Kimura. A numerical method for nonlinear eigenvalue problems using contour integrals. *JSIAM Lett.*, 1:52–55, 2009. doi:10.14495/jsiaml.1.52.
- [3] Marta M. Betcke and Heinrich Voss. Stationary Schrödinger equations governing electronic states of quantum dots in the presence of spin-orbit splitting. *Appl. Math.*, 52:267–284, 2007. doi:10.1007/s10492-007-0014-5.
- [4] Timo Betcke, Nicholas J. Higham, Volker Mehrmann, Christian Schröder, and Françoise Tisseur. NLEVP: A collection of nonlinear eigenvalue problems. *ACM Trans. Math. Software*, 39(2):1–28, 2013. doi:10.1145/2427023.2427024.
- [5] Wolf-Jürgen Beyn. An integral method for solving nonlinear eigenvalue problems. *Linear Algebra Appl.*, 436(10):3839–3863, 2012. doi:10.1016/j.laa.2011.03.030.
- [6] Carmen Campos and Jose E. Roman. NEP: a module for the parallel solution of nonlinear eigenvalue problems in SLEPc. *ACM Trans. Math. Software*, 47(3):1–29, 2021. doi:10.1145/3447544.
- [7] Guillaume Demésy, André Nicolet, Boris Gralak, Christophe Geuzaine, Carmen Campos, and Jose E. Roman. Non-linear eigenvalue problems with GetDP and SLEPc: Eigenmode computations of frequency-dispersive photonic open structures. *Comput. Phys. Commun.*, 257:107509, 2020. doi:10.1016/j.cpc.2020.107509.
- [8] M. Garcia-Vergara, G. Demésy, and F. Zolla. Extracting an accurate model for permittivity from experimental data: hunting complex poles from the real line. *Opt. Lett.*, 42(6):1145–1148, 2017. doi:10.1364/OL.42.001145.
- [9] Walter Gautschi. *Numerical Analysis*. Birkhäuser, New York, NY, USA, 2012. doi:10.1007/978-0-8176-8259-0.
- [10] Brendan Gavin, Agnieszka Międlar, and Eric Polizzi. FEAST eigensolver for nonlinear eigenvalue problems. *J. Comput. Sci.*, 27:107–117, 2018. doi:10.1016/j.jocs.2018.05.006.
- [11] Bo Gong, Jiguang Sun, Tiara Turner, and Chunxiong Zheng. Finite element/holomorphic operator function method for the transmission eigenvalue problem. *Math. Comput.*, 91(338):2517–2537, 2022. doi:10.1090/mcom/3767.
- [12] Stefan Güttel and Françoise Tisseur. The nonlinear eigenvalue problem. *Acta Numer.*, 26:1–94, 2017. doi:10.1017/S0962492917000034.
- [13] Stefan Güttel, Roel Van Beeumen, Karl Meerbergen, and Wim Michiels. NLEIGS: A class of fully rational Krylov methods for nonlinear eigenvalue problems. *SIAM J. Sci. Comput.*, 36(6):A2842–A2864, 2014. doi:10.1137/130935045.
- [14] Varun Hiremath and Jose E. Roman. Acoustic modal analysis with heat release fluctuations using nonlinear eigensolvers. *Appl. Math. Comput.*, 458:128249, 2023. doi:10.1016/j.amc.2023.128249.
- [15] R. Huang, J. Sun, and C. Yang. Recursive integral method with Cayley transformation. *Numer. Linear Algebra Appl.*, 25(6):e2199, 2018. doi:10.1002/nla.2199.

- [16] Ruihao Huang, Allan A. Struthers, Jiguang Sun, and Ruming Zhang. Recursive integral method for transmission eigenvalues. *J. Comput. Phys.*, 327:830–840, 2016. doi:10.1016/j.jcp.2016.10.001.
- [17] Ruihao Huang, Jiguang Sun, and Chao Yang. A multilevel spectral indicator method for eigenvalues of large non-Hermitian matrices. *CSIAM Trans. Appl. Math.*, 1(3):463–477, 2020. doi:10.4208/csiam-am.2020-0021.
- [18] Elias Jarlebring and Siobhán Correnty. Infinite GMRES for parameterized linear systems. *SIAM J. Matrix Anal. Appl.*, 43(3):1382–1405, 2022. doi:10.1137/21M1410324.
- [19] Elias Jarlebring, Wim Michiels, and Karl Meerbergen. A linear eigenvalue algorithm for the nonlinear eigenvalue problem. *Numer. Math.*, 122(1):169–195, 2012. doi:10.1007/s00211-012-0453-0.
- [20] Philipp Jorkowski, Kersten Schmidt, Carla Schenker, Luka Grubišić, and Rolf Schuhmann. Adapted contour integration for nonlinear eigenvalue problems in waveguide coupled resonators. *IEEE Trans. Antennas Propag.*, 70(1):499–513, 2021. doi:10.1109/TAP.2021.3111413.
- [21] Daniel Kressner and Jose E. Roman. Memory-efficient Arnoldi algorithms for linearizations of matrix polynomials in Chebyshev basis. *Numer. Linear Algebra Appl.*, 21(4):569–588, 2014. doi:10.1002/nla.1913.
- [22] Philippe Lalanne, Wei Yan, Alexandre Gras, Christophe Sauvan, J.-P. Hugonin, Mondher Besbes, Guillaume Demésy, M. D. Truong, B. Gralak, F. Zolla, A. Nicolet, F. Binkowski, L. Zschiedrich, S. Burger, J. Zimmerling, R. Remis, P. Urbach, H. T. Liu, and T. Weiss. Quasinormal mode solvers for resonators with dispersive materials. *J. Opt. Soc. Am. A*, 36(4):686–704, 2019. doi:10.1364/JOSAA.36.000686.
- [23] Ruipeng Li, Yuanzhe Xi, Lucas Erlandson, and Yousef Saad. The eigenvalues slicing library (EVSL): Algorithms, implementation, and software. *SIAM J. Sci. Comput.*, 41(4):C393–C415, 2019. doi:10.1137/18M1170935.
- [24] Ben-Shan Liao, Zhaojun Bai, Lie-Quan Lee, and Kwok Ko. Nonlinear Rayleigh-Ritz iterative method for solving large scale nonlinear eigenvalue problems. *Taiwan J. Math.*, 14(3A):869–883, 2010. doi:10.11650/twjm/1500405872.
- [25] Lin Lin, Yousef Saad, and Chao Yang. Approximating spectral densities of large matrices. *SIAM Rev.*, 58(1):34–65, 2016. doi:10.1137/130934283.
- [26] Yuqi Liu, Jose E. Roman, and Meiyue Shao. Improving performance of contour integral-based nonlinear eigensolvers with infinite GMRES. *SIAM J. Sci. Comput.*, to appear.
- [27] Volker Mehrmann and Heinrich Voss. Nonlinear eigenvalue problems: A challenge for modern eigenvalue methods. *GAMM-Mitteilungen*, 27(2):121–152, 2004. doi:10.1002/gamm.201490007.
- [28] André Nicolet, Guillaume Demésy, Frédéric Zolla, Carmen Campos, Jose E. Roman, and Christophe Geuzaine. Physically agnostic quasi normal mode expansion in time dispersive structures: From mechanical vibrations to nanophotonic resonances. *Eur. J. Mech. A Solids*, 100:104809, 2023. doi:10.1016/j.euromechsol.2022.104809.

- [29] Eric Polizzi. Density-matrix-based algorithms for solving eigenvalue problems. *Phys. Rev. B*, 79:115112, 2009. doi:10.1103/physrevb.79.115112.
- [30] Tetsuya Sakurai and Hiroshi Sugiura. A projection method for generalized eigenvalue problems using numerical integration. *J. Comput. Appl. Math.*, 159(1):119–128, 2003. doi:10.1016/S0377-0427(03)00565-X.
- [31] Tetsuya Sakurai and Hiroshi Sugiura. CIRR: a Rayleigh–Ritz type method with contour integral for generalized eigenvalue problems. *Hokkaido Math. J.*, 36(4):745–757, 2007. doi:10.14492/hokmj/1272848031.
- [32] Ziyuan Tang and Yousef Saad. A rational-Chebyshev projection method for nonlinear eigenvalue problems. *Numer. Linear Algebra Appl.*, 31(6):e2563, 2024. doi:10.1002/nla.2563.
- [33] Françoise Tisseur and Nicholas J. Higham. Structured pseudospectra for polynomial eigenvalue problems, with applications. *SIAM J. Matrix Anal. Appl.*, 23(1):187–208, 2001. doi:10.1137/S0895479800371451.
- [34] Lloyd N. Trefethen. Is Gauss quadrature better than Clenshaw–Curtis? *SIAM Rev.*, 50(1):67–87, 2008. doi:10.1137/060659831.
- [35] Roel Van Beeumen. *Rational Krylov Methods and Nonlinear Eigenvalue Problems*. PhD thesis, KU Leuven, 2015.
- [36] Yingxia Xi and Jiguang Sun. Parallel multi-step spectral indicator method for nonlinear eigenvalue problems, 2023. arXiv:2312.13117, doi:10.48550/arXiv.2312.13117.
- [37] Wenqiang Xiao and Jiguang Sun. Band structure calculation of photonic crystals with frequency-dependent permittivities. *J. Opt. Soc. Am. A*, 38(5):628–633, 2021. doi:10.1364/JOSAA.412235.
- [38] Shinnosuke Yokota and Tetsuya Sakurai. A projection method for nonlinear eigenvalue problems using contour integrals. *JSIAM Lett.*, 5:41–44, 2013. doi:10.14495/jsiaml.5.41.